Organic-Soluble Antimicrobial Silver Nanoparticle–Polymer Composites in Gram Scale by One-Pot Synthesis

A. Sreekumaran Nair,[†] Nadappuram P. Binoy,[†] Seeram Ramakrishna,[†] T. R. R. Kurup,[‡] Lai Wah Chan,[‡] Cheong Hian Goh,[‡] Md. Rafiqul Islam,[§] Thomas Utschig,[||] and T. Pradeep*[,||]

Nanoscience and Nanotechnology Initiative, National University of Singapore, Singapore 117576, Department of Pharmacy, National University of Singapore, Singapore 117576, Department of Life Science, Graduate School of Life Science, University of Hyogo, Ako, Hyogo 678-1297, Japan, and DST Unit of Nanoscience, Department of Chemistry and Sophisticated Analytical Instrument Facility, Indian Institute of Technology Madras, Chennai 600036, India

ABSTRACT We report a one-pot synthesis of silver nanoparticle–polymer composites (Ag-PNCs) in water by a novel finding involving the polycondensation of methoxybenzyl chlorides (MeO-BzCl) directly on Ag nanoparticle surfaces at room temperature, leading to highly soluble antimicrobial nanocomposites. The composites, which are soluble in a range of organic solvents, precipitate in the reaction vessel, making their separation simple. Solutions of the composites can be casted directly on substrates or made into freestanding films. The material was found to be stable for nearly 2 years. A range of substrates have been shown to become antibacterial by direct application of this material. The experiments were conducted with Ag-PNC-loaded filter paper strips and glass substrates. The samples were found to be antimicrobial (against *Escerichia coli* and *Aspergillus niger*). The simple one-pot approach of this kind to make organic-soluble antibacterial coatings could have wide implications.

KEYWORDS: silver nanoparticles • methoxybenzyl chlorides • polycondensation • nanoparticle–polymer composites • antimicrobial

INTRODUCTION

The utility of metal nanoparticles as reagents/catalysts in chemistry has tremendous potential in organic synthesis and materials science (1–3). Nanoparticle–polymer composites prepared by single-step and multistep methodologies have advantageous optical, electrical, and mechanical properties and have found widespread applications in catalysis, health care, bioengineering, photonics, and electronics (4). Nanosilver is a versatile antimicrobial agent (5) and is an excellent substrate for surface-enhanced Raman scattering (SERS) (6) and metal-enhanced fluorescence (7). Synthesis of silver nanoparticle–polymer composites (Ag-PNCs) by simple and efficient methodologies provides tremendous opportunities in the ever-expanding markets of polymer nanocomposites (8). We note that the current global consumption of polymer nanocomposites is worth ~$250 million with a potential annual growth rate of 24%, and the demand is expected to reach $500–800 million in 2011 (8).

Water-soluble Ag-PNCs could be synthesized by green methodologies using polysaccharides as reducing and capping agents (9). However, the weak binding interactions between Ag and the polymers usually lead to phase separation of the components. Several bio-organisms were also used as reducing and/or capping agents in the syntheses of water-soluble Ag-PNCs (10). However, there exist limited methods for the synthesis of organic-soluble Ag-PNCs (11). Commonly adopted physical and chemical methods for the syntheses of Ag-PNCs are the dispersion of previously prepared nanoparticles in a polymer matrix (12), in situ synthesis of nanoparticles in the polymer matrix (13), and simultaneous metal reduction and polymerization (14). However, inhomogeneous distribution of nanoparticles, the absence of solubility and repeated redispersibility in solvents, cumbersome synthetic procedures, and the absence of demonstrable antimicrobial nature have contributed to poor applications for the composites (4f, 15).

Here we report a novel one-pot methodology of synthesizing antimicrobial Ag-PNCs by Ag nanoparticle catalyzed polycondensation of methoxybenzyl chlorides in a water–isopropyl alcohol mixture at room temperature. The Ag-PNCs formed precipitate from the reaction mixture but are freely soluble in common organic solvents and could be stored for extended periods in solid form or as solutions without losing physical or chemical characteristics of the embedded nanoparticles. To the best of our knowledge, the polycondensation of the monomers on the surfaces of Ag nanoparticles is an absolutely novel and simple methodology to synthesize Ag-PNCs at room temperature.

* To whom correspondence should be addressed. E-mail: pradeep@iitm.ac.in. Tel: +91-44-22574208.
Received for review July 29, 2009 and accepted October 27, 2009
[†] Nanoscience and Nanotechnology Initiative, National University of Singapore.
[‡] Department of Pharmacy, National University of Singapore.
[§] University of Hyogo.
[||] Indian Institute of Technology Madras.
DOI: 10.1021/am9005034

EXPERIMENTAL SECTION

(a) Synthesis of Ag@citrate. $AgNO_3$, trisodium citrate dihydrate, and 2-propanol were obtained from Wako Pure Chemicals (Japan) and were used as received. 2-Methoxy- and 4-methoxybenzyl chloride (MeO-BzCl) and sodium borohydride ($NaBH_4$) were purchased from Aldrich and used as received. Distilled water (resistivity >18 MΩ cm), obtained from an Advantec GS-200 automatic water distillation apparatus, was used for the reactions. Citrate-capped Ag nanoparticles (~4 nm, abbreviated as Ag@citrate in further discussions below) were synthesized by the $NaBH_4$ reduction method. As per the procedure, 10 mL of 10^{-2} M $AgNO_3$ was mixed with 10 mL of 10^{-2} M trisodium citrate solution (in water) at room temperature. The mixture was diluted to 390 mL using distilled water. Ten milliliters of a 0.1 M ice-cooled solution of $NaBH_4$ was then added dropwise (at a rate of 120 mL/h using a syringe pump) to the above solution with stirring. The solution became golden yellow. The Ag nanoparticles thus produced have an absorption maximum at 382 nm, corresponding to an average particle diameter of ~4 nm. The size, size distribution, and shape of the nanoparticles were additionally confirmed by a high-resolution transmission electron microscope (HR-TEM). The nanoparticle solution was checked for the presence of free Ag^+ ions, and the absence of them confirmed that the reduction was complete.

(b) Silver Nanoparticle−Polymer Composites (Ag-PNCs) by Polycondensation. The procedure for the synthesis of silver−polymer nanocomposites (Ag-PNCs) was as follows: a 200 mL portion of the as-prepared Ag@citrate nanoparticles was added to 300 mL of 2-propanol in a round-bottom flask, and the mixture was stirred for about 5 min for homogeneity. Two milliliters of 2-MeO-BzCl or 4-MeO-BzCl was then added to the nanoparticle−2-propanol mixture dropwise with stirring. The golden yellow color of the nanoparticle solution slowly changed to brownish yellow over a period of ~6 h, and finally a reddish brown residue precipitated (~12 h). The residue was separated by centrifugation and washed with water and 2-propanol several times. The precipitate was then washed with 25% NH_3 (with sonication) to remove adsorbed AgCl (a part of the Ag gets converted to AgCl during the polycondensation reaction and lies attached to the polymer) on the polymer (XRD of the sample was taken before NH_3 wash as we wanted to see the AgCl peaks in the XRD) and again with 2-propanol and then freeze-dried. The freeze-dried material was soluble in organic solvents such as benzene, toluene, chlorobenzene, dichloromethane, chloroform, tetrahydrofuran, dimethylformamide, and dimethyl sulfoxide. Freeze-dried powders and their solutions in benzene or toluene were used for characterization by spectroscopy and microscopy.

(c) Characterization Methods. Absorption spectra (in respective solvents) were measured using a Perkin-Elmer Lambda 25 UV−visible spectrometer and a Hitachi U-4100 spectrophotometer. Transmission electron micrographs were taken using a Hitachi H-8100 electron microscope operating at 200 kV and a JEOL 3010 UHR transmission electron microscope (TEM) operating at 300 kV. A drop of the solution was cast on a carbon-coated copper grid, and the solution was allowed to evaporate under ambient conditions. The grid was then subjected to vacuum overnight and used for TEM measurements. Fourier transform infrared (FT-IR) spectra were acquired with a Perkin-Elmer Spectrum One spectrometer. Spectra of pure MeO-BzCl were measured in a standard liquid cell. Spectra of Ag-PNCs were measured using a KBr pellet having 5% of the vacuum-dried materials. Raman spectra of the Ag-PNCs (solutions were drop-casted and evaporated on cover glass slides) were acquired with a CRM 200 Confocal Raman spectrometer (Witec, Germany). Raman spectra of pure MeO-BzCl were measured by taking the samples in a glass capillary. XRD measurements (concentrated solutions of the materials were drop-casted on standard cavity mounts and dried) were taken with a Rigaku RINT/DMAX-2000 X-ray diffractometer with Cu Kα radiation (40 kV, 20 mA). Nuclear magnetic resonance (NMR) spectra (in C_6D_6 solvent) were recorded with a JEOL (AS-600) 600 MHz multinuclei FT-NMR instrument. X-ray photoelectron spectra were measured using an ESCA probe from Omicrometer Nanotechnology. Al Kα radiation was used for excitation, and a 180° hemispherical analyzer and a seven-channel detector were employed. The pressure in the analyzer chamber was on the level of 10^{-10} mbar during spectra collection. Thermogravimetric (TG) data were acquired with a Netzsch STA 409C instrument. Data in the range 28−1200 °C were measured under an N_2 atmosphere. A scan speed of 10 °C/min was used in these measurements. The pH changes during the course of the reaction were measured using a conventional instrument.

(d) Antimicrobial Tests. Antimicrobial properties of Ag-PNCs were tested against *Escherichia coli* (ATCC 8739, gram negative) and *Aspergillus niger* (ATCC 16404) strains procured from the American Type Culture Collection (ATCC, The Global Bioresource Center). Nutrient agar was obtained from Oxoid Limited (U.K.). Antimicrobial tests were done as per standard protocols, as explained in the appropriate section below.

RESULTS AND DISCUSSION

Polycondensation of benzyl chlorides is an electrophilic aromatic polysubstitution process generally catalyzed by some metal halides and group VIB and VIIB carbonyls (16, 17). We have found that water-soluble Ag@citrate also facilitates polycondensation of MeO-BzCl on Ag nanosurfaces in a water−isopropyl alcohol mixture, resulting in organic-soluble Ag-PNCs. This is a novel finding, as the monomers are polymerized at the Ag nanoparticle surfaces at room temperature without the help of any external catalyst. The amount of Ag-PNC formed from one typical synthesis was ~13 mg (after freeze-drying). Polybenzyls are insoluble in solvents such as hexane (while the monomers are soluble) but are freely soluble in benzene, toluene, chlorobenzene, dichloromethane, and chloroform. The Ag-PNCs in the present case also exhibited the same selective solubility. The saturation solubility of the material in toluene was found to be ~1.2 g/mL. In terms of Ag content, this corresponds to 122 mg/mL. We believe that the halogenophilicity of the Ag nanoparticles (18) facilitates adsorption of MeO-BzCl on the surfaces, which further drives the polycondensation reaction through a carbocation mechanism (see below).

(a) Characterization of Ag-PNCs. Figure 1 shows the UV−visible spectra of Ag@citrate (trace a) and the Ag-PNCs (in toluene medium) formed from 4-MeO-BzCl (trace b) and 2-MeO-BzCl (trace c), respectively. The UV−visible spectrum of the Ag@citrate shows the surface plasmon resonance at 382 nm, characteristic of the ~ 4 nm particles. The peak maxima of Ag-PNCs in traces b and c are 417 and 425 nm, respectively. The red-shift as well as the increase in the width of the surface plasmon peak of Ag in the Ag-PNCs compared to that of the parent Ag@citrate is due to the effect of the dielectric constant of the polymer matrix in which the nanoparticles are embedded (19) and an increase in the size of the nanoparticles (20) (see the TEM images, below). Inset in Figure 1 shows a view of the freeze-dried Ag-PNC, which could be stored of the order of tens of months

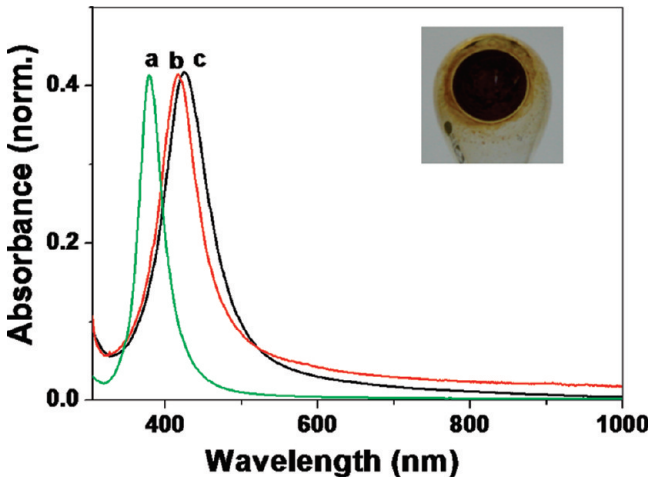

FIGURE 1. UV−visible spectra of (a) citrate-capped Ag nanoparticles and Ag-PNCs formed from (b) 4-MeO-BzCl and (c) 2-MeO-BzCl, respectively. The surface plasmon peak of ~4 nm Ag@citrate is at 382 nm, and those for Ag-PNCs are at 417 and 425 nm, respectively. The inset shows a picture of the freeze-dried Ag-PNC from 2-MeO-BzCl in a round-bottom flask.

without any physical or chemical changes to the nanoparticles. We have tested the samples for two years.

Figure 2A shows the color of the Ag@citrate (golden yellow, left) used for Ag-PNC synthesis and the Ag-PNC (in toluene medium) formed from 2-MeO-BzCl (reddish brown, right). The color of the concentrated solution (note that there is a reduction in volume by a factor of 40 in the composite solution) of the Ag-PNC is due to the combined effect of the higher dielectric constant of the polymer matrix and the decreased interparticle distance between the nanoparticles in the composite in comparison to the parent Ag@citrate particles (20). Figure 2B−D shows thin films of Ag-PNC fabricated on a glass plate, a filter paper disk, and a metal plate, respectively, using dip-coating, demonstrating the flexibility of the material for surface coatings and thin films.

The Ag@citrate particles used for Ag-PNC syntheses and the Ag-PNCs formed were characterized using transmission electron microscopy (TEM). In Ag@citrate, most of the particles were of ~4 nm diameter and were spherical in geometry with a few elongated and much smaller particles (Supporting Information, Figure S1). The TEM images of the Ag-PNCs formed from 4-MeO-BzCl and 2-MeO-BzCl are shown in Figure 3. Figure 3A gives the Ag-PNC formed from 4-MeO-BzCl, showing the presence of Ag nanoparticles in the polymer matrix. Figure 3B is an HR-TEM image of the periphery of a nanoparticle in the composite showing the polymer shell around it. Figure 3C is the TEM of the Ag-PNC formed from 2-MeO-BzCl, showing the nanoparticles embedded in the polymer matrix. Figure 3D gives a TEM image of a nanoparticle, showing its proximity to the polymer matrix. Its inset represents a high-resolution image showing the (111) lattice spacing of Ag. The presence of Moiré fringes in the nanoparticle indicates its polycrystalline nature. The presence of the polymer layer around the particles imparts long term stability and repeated redispersibility to the Ag-PNCs without affecting the physical and chemical characteristics of the nanoparticles. It should be noted that the average sizes of the nanoparticles in both the Ag-PNCs (~20 nm) are larger than those of the nanoparticles used for the reaction (~4 nm). This is because of the adsorbate (MeO-BzCl)-induced aggregation (18, 21) of the nanoparticles during the course of the polycondensation reaction. This was further confirmed by a time-dependent UV−visible study (Supporting Information, Figure S2) of the interaction of MeO-BzCl with the Ag nanoparticles at the initial stages of the polycondensation reaction (taken at 5 min intervals, up to 30 min), which showed a reduction in the intensity of the original surface plasmon peak and the emergence of another broad plasmon feature at longer wavelengths, which is a clear indication of the adsorbate-induced aggregation of the nanoparticles. The very small particles observed in the Ag@citrate (see Figure S1 in the Supporting Information) were not seen in the composite, and this could be because of the Ostwald ripening process.

The Ag-PNCs formed were further characterized by infrared and Raman spectroscopy, X-ray diffraction, ^{1}H NMR, and X-ray photoelectron spectroscopy (XPS) (Supporting Information, Figures S3−S7). Infrared spectra of the monomers and the Ag-PNCs (Supporting Information, Figure S3) showed the disappearance of the C−Cl features of MeO-BzCl (657 cm^{-1}, sym C−Cl stretch; 724 cm^{-1}, asym C−Cl stretch) in the nanocomposites due to the polycondensation reaction. Raman spectra (Supporting Information, Figure S4) also showed similar features. The IR and Raman features of the polymers in the composites showed slight shifts from those of pure MeO-BzCl, owing to their proximity to the nanosurfaces. X-ray diffraction of the thin films of the nanocomposites (before NH_3 wash; Supporting Information, Figure S5) showed diffraction from (111), (200), and (220) planes of Ag in addition to a peak for AgCl assigned to (200). The peaks due to AgCl disappeared upon NH_3 wash, as expected. The average size of the particles estimated from the XRD line broadening using the Scherer formula was ~22 nm, in close agreement with TEM observations. The presence of the polymer in the composite was also confirmed by a ^{1}H NMR study. A comparison of the NMR spectra of 2-MeO-BzCl and the Ag-PNC formed from the same (traces A and B, respectively, in Figure S6 of the Supporting Information) showed that the peaks get broadened in the latter. The features in Ag-PNC occur at δ_H 7.1−6.5, 3.2, and 4.1 ppm, corresponding to −Ph, −OMe, and −CH_2. The XPS survey spectrum and scans in the various core level regions are consistent with the chemical structure (Supporting Information, Figure S7). The thermal stability of the polymers was investigated by thermogravimetry (Supporting Information, Figure S8). For the Ag-PNCs formed from both 4-MeO-BzCl and 2-MeO-BzCl, the polymers were stable up to 320 °C, and thereafter they degrade. The composites retain ~38% of the mass even at 1200 °C.

(b) Mechanism of Polycondensation. A general schematic of the Ag nanoparticle catalyzed polycondensation is shown in Scheme 1. As mentioned previously, the polycondensation in the present case results from the halogenophilicity of the Ag nanoparticles. MeO-BzCl adsorbs on

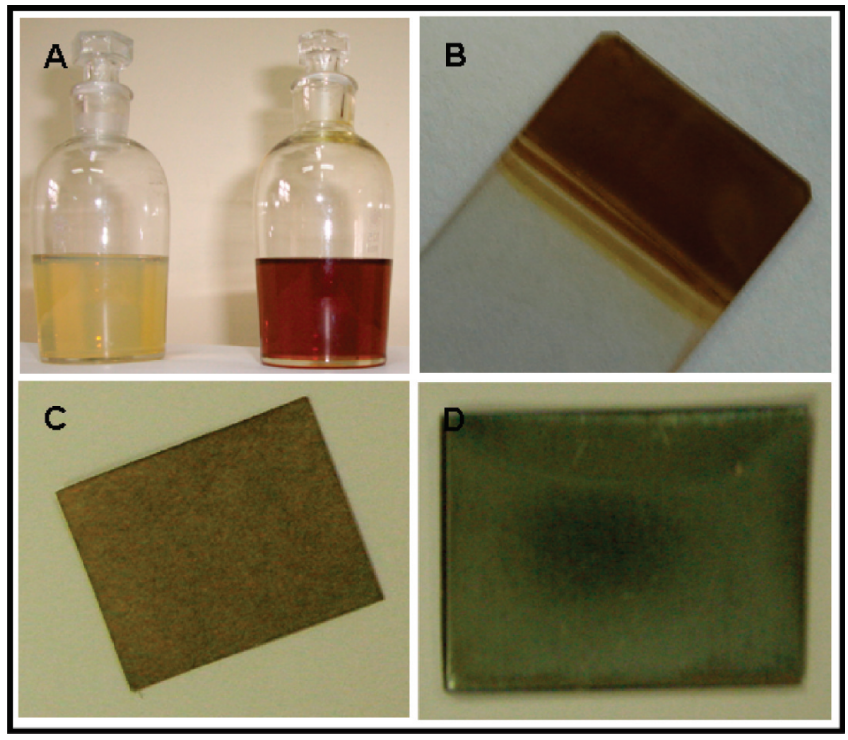

FIGURE 2. (A) The color of Ag@citrate (golden yellow, left) used for the Ag-PNC synthesis and the Ag-PNC (in toluene medium, right) synthesized from 2-MeO-BzCl. (B−D) images of thin films of the Ag-PNC fabricated on glass, a filter paper strip, and a metal sheet, respectively, by dip-coating.

the surfaces of the Ag nanoparticles (see the time-dependent UV−visible study mentioned earlier in Figure S2 of the Supporting Information), and subsequent halide abstraction (a part of the Ag gets converted into AgCl (22), as was seen from the XRD of the Ag-PNCs) generates carbonium ion (steps A and B in the scheme), which stabilizes via resonance on the phenyl ring. The presence of an −OMe group in the phenyl ring further facilitates generation of carbonium ions on the nanosurfaces. The carbonium ions then react with methoxybenzyl chlorides to produce primarily benzyl isomers of ortho (to the methoxy group in the case of 4-MeO-BzCl) and para (to the methoxy group in the case of 2-MeO-BzCl) substituted bis(methoxyphenyl)methane (step D). As the polycondensation proceeds, the generated oligomers provide more feasible benzene rings for attack by the carbonium ions, resulting in the formation of polymers (step E). The polymer formed by the polycondensation process remains attached to the surfaces of the nanoparticles (catalyst) because of the insoluble nature of the polymer in the solvent mixture (water−isopropyl alcohol mixture). This is expected to deactivate the catalyst surfaces due to the occupation of the catalytically active sites. The protons released during the polycondensation process are responsible for the decrease of pH of the medium from 11.0 (that of the Ag@citrate−isopropyl alcohol mixture) to 1.70 (pH of the supernatant after the polycondensation). No attempt was made to find the molecular weight of the polymers, as the polydisperse nanoparticles catalyze the polycondensation reaction to varying extents, resulting in a mixture of polymers having different molecular weights in the Ag-PNCs. The reaction was also found to occur with 1-propanol, ethanol, and methanol instead of 2-propanol. A control experiment of MeO-BzCl with the same quantity of $AgNO_3$ (instead of Ag nanoparticles) in the presence of a H_2O−isopropyl alcohol mixture did not give any polymer. This confirmed that the polycondensation of MeO-BzCl is indeed catalyzed by the surfaces of the Ag nanoparticles. Other noble metal nanoparticles of gold and copper did not bring about the polycondensation of MeO-BzCl, indicating that the reaction is specific to the surfaces of Ag nanoparticles (23). The exact mechanistic aspects of the polycondensation on single Ag nanocrystals could be unraveled using surface plasmon spectroscopy (a similar attempt to directly observe chemical reactions on single nanocrystals was reported recently) (24), which could be be investigated in the future.

(c) Antimicrobial Activity of Ag-PNCs. The antimicrobial nature of Ag-PNCs was investigated using the "disk diffusion qualitative assay method". The materials are highly soluble in benzene, toluene, CCl_4, etc., but the solvents themselves are antibacterial. Therefore, the more accurate "multiple serial dilution methodology" was not adopted in the present case. The composites exhibited good antimicrobial activity. The sample obtained from one typical synthesis (after NH_3 treatment to remove AgCl and a subsequent wash with water and ethanol, respectively) was freeze-dried and dissolved in 3 mL of toluene. Portions of the above solution (10, 20, and 50 μL) were placed on three filter paper disks (of area ~10 mm^2, labeled 1−3 in Figure 4A). The fourth disk was kept in the Ag-PNC solution overnight for saturated loading of the composite material. A control disk (labeled 5 in Figure 4) soaked in toluene was also processed under similar conditions. The disks were then kept in a fume hood

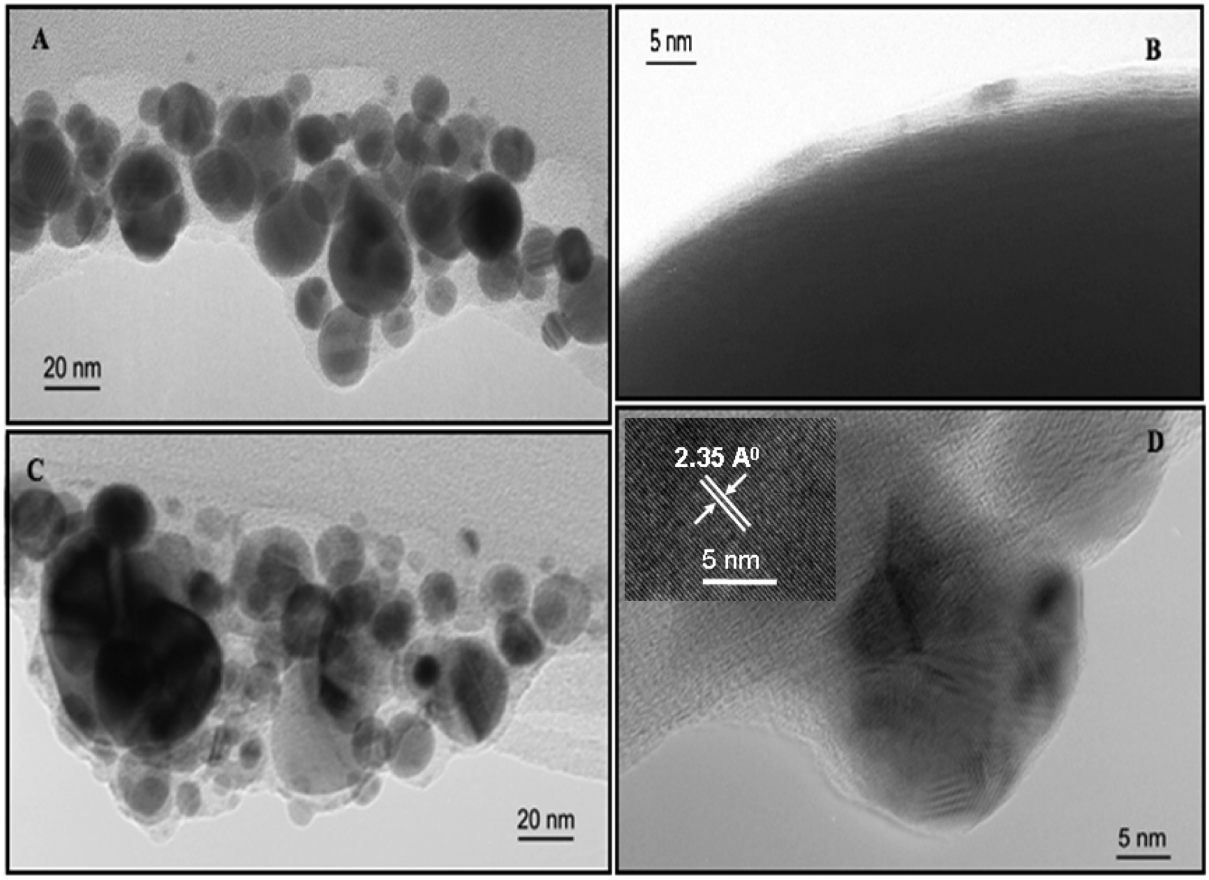

FIGURE 3. TEM images of the Ag-PNCs formed from 4-MeO-BzCl (A and B) and 2-MeO-BzCl (C and D). The large area image A shows the Ag nanoparticles embedded in the polymer matrix. Polydispersity is common for silver, as is evident from the TEM image. Image B is a high-resolution image of a nanoparticle of the composite, showing the presence of a thin polymer matrix around the nanoparticle. (C) TEM image of the Ag-PNCs from 3-MeO-BzCl, showing the nanoparticles in the polymer matrix. (D) HRTEM image of a nanoparticle in the polymer matrix. The Ag(111) lattice can be seen in an expanded image in the inset.

Scheme 1. Polycondensation Reaction of MeO-BzCl on Ag Nanosurfaces

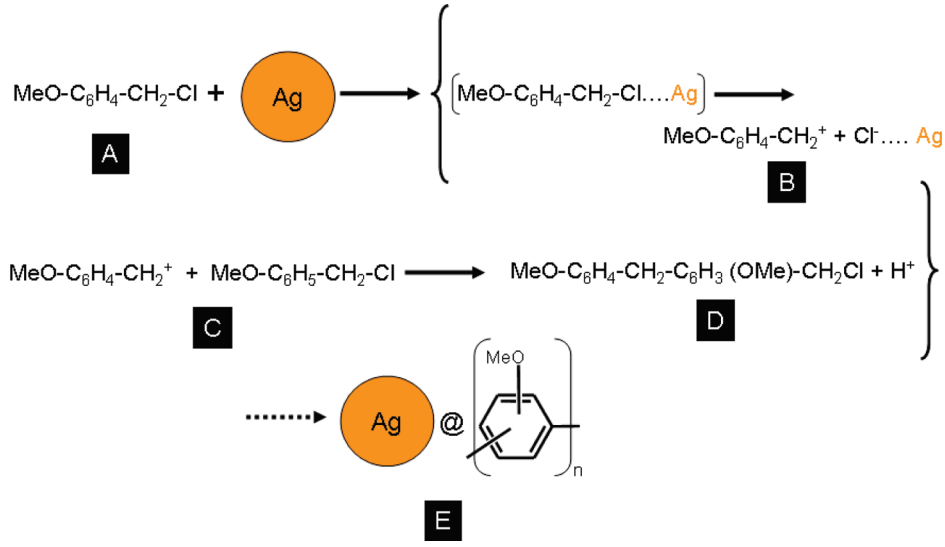

overnight so as to completely evaporate toluene. The perfectly dried disks were used for antimicrobial studies. These disks were aseptically applied to the surface of agar plates having 200 μL of *E. coli* (of 24 h culture, 10^6 CFU/mL) spread uniformly. The plates were incubated at 37 °C for 24 h, and the zones of inhibition were measured. All the disks except the control showed nearly the same width of zones of inhibition of 2.3 mm. This implies that the nano Ag in the Ag-PNCs was active against *E. coli*. The amount of atomic Ag in the 10 μL Ag-PNC loaded disk (the one with the lowest amount of Ag) was ~16 μg. The lowest concentration of Ag at which the zone of inhibition was visible was ~3 μg/disk. The plates stored at 37 °C were further observed for several weeks. It is important to mention that the observed anti-

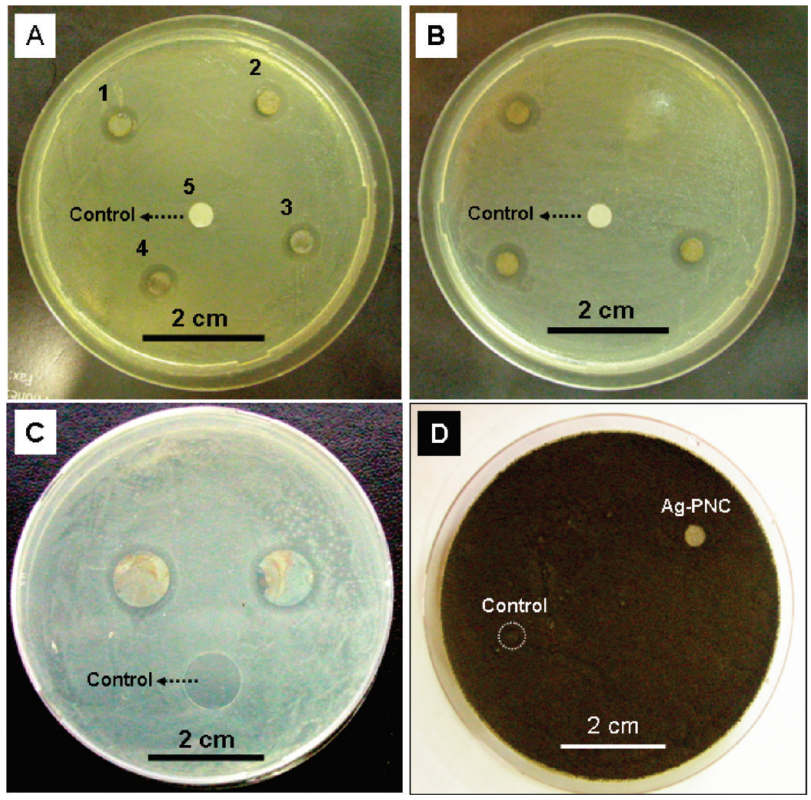

FIGURE 4. Antibacterial tests with *E. coli* strains on Ag-PNCs coated on filter paper disks (A and B) and glass plates (C). The zone of inhibition is very clear from the images. Image D shows an antifungal test against *Aspergillus niger*.

bacterial activity is static, as the clear zone of inhibition persisted for several months (a slight increase in the width was observed over a period of time) under observation. To confirm the reproducibility of the results, we have performed the experiments with three disks having saturately loaded Ag-PNCs (Figure 4B). The width of zone of inhibition was found to be nearly the same for all three disks (~ 2.5 mm). The materials coated on glass slides also showed similar antibacterial activities (Figure 4C). It should be noted that the antibacterial activity of nano Ag depends on its size and shape (25). In previous reports, bamboo charcoal adsorbed Ag nanoparticles (35−100 nm size prepared by chemical reduction routes), protein-capped Ag nanoparticles (~ 22 nm) synthesized by bacterial reduction, sodium dodecyl sulfate (SDS)-capped Ag nanoparticles (~ 45 nm), uncapped Ag nanoparticles (~ 3 nm), and citrate-capped Ag nanoparticles (~12 nm) were used for antibacterial studies (26) by the zone of inhibition method. They showed widths of the zone of inhibition of ~12 mm (the concentration of Ag was 6 mg/mL per disk), ~9 mm (Ag load of 10 μg/disk), ~6 mm (5 μg Ag/disk), and ~14 mm (Ag load of 100 μg/disk), respectively. Even for citrate-capped Ag nanoparticles (~12 nm size); the bactericidal concentration was 25 μg/disk (26e). A comparison of the zone of inhibition widths in the present case with those in the literature (having comparable sizes of the nanoparticles) indicates that the bactericidal action of the Ag-PNCs is promising. The width of zone of inhibition observed in the present case was slightly smaller compared to that of proteins and SDS-capped Ag nanoparticles (hydrophilic), and this could be because of the hydrophobic nature of the Ag-PNCs in the present case, which restricts the diffusion of the Ag nanoparticles into the hydrophilic growth medium. Additionally, SDS is an ionic surfactant and may have the ability to penetrate and/or disrupt the bacterial cell wall and the bactericidal action of the material could be because of the combined effect of nano Ag and the SDS (25c). A direct comparison of the antibacterial results of the present material with those in the literature may not, therefore, be appropriate.

We have further checked whether the Ag-PNCs are active against fungi as well. Separate experiments were done with *Aspergillus niger* (with a spore load of 10^6 CFU/mL) and a mixture of several fungi recovered from the wall of a building. The plates were observed after 2 weeks of incubation. While there was growth of fungi for the control in both cases (note that the control is not even visible due to fungi growth over them), the same was not seen for the disks having the Ag-PNCs (Supporting Information, Figure S9). This implies that the Ag-PNCs could also resist the growth of fungi. The fact that the Ag-PNCs are freely soluble even at very high concentrations in organic solvents makes them excellent candidates for hydrophobic surface coatings and provides enormous flexibility in devising thin films on various substrates.

CONCLUSIONS

A novel one-pot route for the syntheses of Ag-PNCs at room temperature is presented. Ag nanoparticle surfaces catalyze the polycondensation of methoxybenzyl chlorides in H_2O−isopropyl alcohol mixtures, resulting in nanopar-

ticle−polymer composites. The nanocomposites were thoroughly characterized by UV−visible, TEM, IR, Raman, ^{1}H NMR, XRD, XPS, and thermogravimetry analyses. The nanocomposites were stable and could be stored in solid and solution forms for extended periods without any chemical or physical changes to the nanoparticles. The Ag-PNCs are highly soluble and showed good antimicrobial activity. We anticipate applications for the nanocomposites in areas such as high-temperature adhesives, coatings, antibacterial paints, varnishes, textiles, health care, and defense.

Acknowledgment. The nanoparticle research program of T.P. is supported by the Department of Science and Technology. Most of this work was completed when A.S.N. was at the Indian Institute of Technology Madras.

Supporting Information Available: Text and figures giving details of the TEM images of ~4 nm Ag@citrate, time-dependent UV−visible spectra of the polycondensation reaction, infrared, Raman, and NMR spectra of the monomers and Ag-PNCs, and the XRD, XPS, and TG traces of Ag-PNCs. This material is available free of charge via the Internet at http://pubs.acs.org.

REFERENCES AND NOTES

(1) Chen, M. S.; Goodman, D. W. *Science* **2004**, *306*, 252–255.

(2) Astruc, D.; Lu, F.; Aranzaes, J. R. *Angew. Chem., Int. Ed.* **2005**, *44*, 7852–7872.

(3) (a) Walters, G.; Parkin, I. P. *J. Mater. Chem.* **2009**, *19*, 574–590. (b) Astruc, D. *Inorg. Chem.* **2007**, *46*, 1884–1894.

(4) (a) Baur, J.; Silverman, E. *MRS Bull.* **2007**, *32*, 328–334. (b) Winey, K. I.; Kashiwagi, T.; Mu, M. *MRS Bull.* **2007**, *32*, 348–353. (c) Hule, R. A.; Pochan, D. J. *MRS Bull.* **2007**, *32*, 354–358. (d) Chu, H. Y. V.; Liu, Y.; Huang, Y.; Zhao, Y. *Opt. Express* **2007**, *15*, 12230–12239. (e) Kumar, V. R. R.; Samal, A. K.; Sreeprasad, T. S.; Pradeep, T. *Langmuir* **2007**, *23*, 8667–8669. (f) Kumar, V. R. R.; Pradeep, T. *J. Mater. Chem.* **2006**, *16*, 837–841.

(5) (a) Balogh, L.; Swanson, D. R.; Tomalia, D. A.; Hagnauer, G. L.; McManus, A. T. *Nano Lett.* **2001**, *1*, 18–21. (b) Jain, P.; Pradeep, T. *Biotechnol. Bioeng.* **2005**, *90*, 59–63.

(6) (a) Aslan, K.; Leonenko, Z.; Lakowicz, J. R.; Geddes, C. D. *J. Fluoresc.* **2005**, *15*, 643–654. (b) Matveeva, E.; Gryczynski, Z.; Malicka, J.; Gryczynski, I.; Lakowicz, J. R. *Anal. Biochem.* **2004**, *334*, 303–311.

(7) Baker, G. A.; Moore, D. S. *Anal. Bioanal. Chem.* **2005**, *382*, 1751–1770.

(8) (a) McWilliams, A. NANO21C; BBC Research, Norwalk, CT, 2006. (b) Thayer, A. M. *Chem. Eng. News* **2000**, *78*, 36–38.

(9) (a) Raveendran, P.; Fu, J.; Wallen, S. L. *J. Am. Chem. Soc.* **2003**, *125*, 13940–13941. (b) Raveendran, P.; Fu, J.; Wallen, S. L. *Green Chem.* **2006**, *8*, 34–38. (c) Huang, H.; Yang, X. *Carbohydr. Res.* **2004**, *339*, 2627–2631. (d) Vigneshwaran, N.; Nachane, R. P.; Balasubramanya, R. H.; Varadarajan, P. V. *Carbohydr. Res.* **2006**, *341*, 2012–2018. (e) Sato, Y.; Wang, J. J.; Batchelder, D. N.; Smith, D. A. *Langmuir* **2003**, *19*, 6857–6861. (f) Libor, K.; Robert, P.; Aleš, P.; Radko, N.; Jan, H.; Radek, Z. *J. Mater. Chem.* **2005**, *15*, 1099–1105. (g) Panáček, A.; Kvı´tek, L.; Prucek, R.; Kolář, M.; Večeřŏvá, R.; Pizúrová, N.; Sharma, V. K.; Nevečňá, T.; Zboril, R. *J. Phys. Chem. B* **2006**, *110*, 16248–16253.

(10) (a) Xie, J.; Lee, J. Y.; Wang, D. I. C.; Ting, Y. P. *ACS Nano* **2007**, *1*, 429–439. (b) Gardea-Torresdey, J. L.; Gomez, E.; Peralta-Videa, J. R.; Parsons, J. G.; Troiani, H.; Jose-Yacaman, M. *Langmuir* **2003**, *19*, 1357–1361. (c) Shankar, S. S.; Ahmad, A.; Sastry, M. *Biotechnol. Prog.* **2003**, *19*, 1627–1631.

(11) (a) Lee, K. J.; Jun, B. H.; Choi, J.; Lee, Y.; Joung, J.; Oh, Y. S. *Nanotechnology* **2007**, *18*, 33560. (1−5). (b) Singh, N.; Khanna, P. K. *Mater. Chem. Phys.* **2007**, *104*, 367–372.

(12) (a) Korchev, A. S.; Bozack, M. J.; Slaten, B. L.; Mills, G. *J. Am. Chem. Soc.* **2004**, *126*, 10–11. (b) Zheng, M.; Gu, M.; Jin, Y.; Jin, G. *Mater. Res. Bull.* **2001**, *36*, 853–859. (c) Vimala, K.; Sivudu, K. S.; Mohan, Y. M.; Sreedhar, B.; Raju, K. M. *Carbohydr. Polym.* **2009**, *75*, 463–471. (d) Sawada, H.; Sasaki, A.; Sasazawa, K.; Toriba, K.; Kakehi, H.; Miura, M.; Isu, N. *Polym. Adv. Technol.* **2008**, *19*, 419–424. (e) Eksik, O.; Erciyes, A. T.; Yagci, Y. *J. Macromol. Sci., Pure Appl. Chem.* **2008**, *45*, 698–704. (f) Sanpui, P.; Murugadoss, A.; Prasad, P. V. D.; Ghosh, S. S.; Chattopadhyay, A. *Int. J. Food Microbiol.* **2008**, *124*, 142–146.

(13) (a) Saquing, C. D.; Manasco, J. L.; Khan, S. A. *Small* **2009**, *5*, 944–951. (b) Thomas, V.; Yallapu, M. M.; Sreedhar, B.; Bajpai, S. K. *J. Appl. Polym. Sci.* **2009**, *111*, 934–944. (c) Perkas, N.; Shuster, M.; Amirian, G.; Koltypin, Y.; Gedanken, A. *J. Polym. Sci., Part A: Polym. Chem.* **2008**, *46*, 1719–1729. (d) Bakumov, V.; Gueinzius, K.; Hermann, C.; Schwarz, M.; Kroke, E. *J. Eur. Ceram. Soc.* **2007**, *27*, 3287–3292.

(14) Akamatsu, K.; Ikeda, S.; Nawafune, H. *Langmuir* **2003**, *19*, 10366–10371.

(15) (a) Pintér, E.; Patakfalvi, R.; Fülei, T.; Gingl, Z.; Dékány, I.; Visy, C. *J. Phys. Chem. B* **2005**, *109*, 17474–17478. (b) Hasell, T.; Thurecht, K. J.; Jones, R. D. W.; Brown, P. D.; Howdle, S. M. *Chem. Commun.* **2007**, 3933–3935. (c) Oliveira, M. M.; Castro, E. G.; Canestraro, C. D.; Zanchet, D.; Ugarte, D.; Roman, L. S.; Zarbin, A. J. G. *J. Phys. Chem. B* **2006**, *110*, 17063–17069. (d) Mbhele, Z. H.; Salemane, M. G.; van Sittert, C. G. C. E.; Nedeljkoviæ, J. M.; Djokoviæ, V.; Luyt, A. S. *Chem. Mater.* **2003**, *15*, 5019–5024. (e) Manna, S.; Batabyal, S. K.; Nandi, A. K. *J. Phys. Chem. B* **2006**, *110*, 12318–12326.

(16) (a) Jacobson, R. A. *J. Am. Chem. Soc.* **1932**, *54*, 1513–1518. (b) Dermer, O. C.; Hooper, E. *J. Am. Chem. Soc.* **1941**, *63*, 3525–3526. (c) Kuo, J.; Lenz, R. W. *J. Polym. Sci., Polym. Chem. Ed.* **1976**, *14*, 2749–2761. (d) Spanier, E. J.; Caropreso, F. E. *J. Polym. Sci., Part A1* **1969**, *7*, 2679–2687.

(17) (a) Tsonis, C. P. *Polym. Bull.* **1983**, *9*, 349–354. (b) Tsonis, C. P. *J. Mol. Catal.* **1990**, *57*, 313–323. (c) Choudhary, V. R.; Jana, S. K.; Chaudhari, M. K. *J. Mol. Catal. A: Chem.* **2001**, *170*, 251–259.

(18) (a) Henglein, A. *Chem. Mater.* **1998**, *10*, 444–450. (b) Nair, A. S.; Pradeep, T. *Curr. Sci.* **2003**, *84*, 1560–1564. (c) Nair, A. S.; Tom, R. T.; Suryanarayan, V.; Pradeep, T. *J. Mater. Chem.* **2003**, *13*, 297–300. (d) Suryanarayan, V.; Nair, A. S.; Tom, R. T.; Pradeep, T. *J. Mater. Chem.* **2004**, *14*, 2661–2666.

(19) Ung, T.; Liz-Marzán, L. M.; Mulvaney, P. *J. Phys. Chem. B* **2001**, *105*, 3441–3452.

(20) (a) Kelly, K. L.; Coronado, E.; Zhao, L. L.; Schatz, G. C. *J. Phys. Chem. B* **2003**, *107*, 668–677. (b) Charlé, K. P.; Schulze, W.; Winter, B. *Z. Phys. D: At. Mol. Clusters* **1989**, *12*, 471–475.

(21) (a) Nair, A. S.; Tom, R. T.; Pradeep, T. *J. Environ. Monitor.* **2003**, *5*, 363–365. (b) Nair, A. S.; Pradeep, T. *J. Nanosci. Nanotechnol.* **2007**, *7*, 1871–1877.

(22) The fact that the AgCl lies attached to the Ag-PNCs surfaces further implies the formation of AgCl from the surfaces of the nanoparticles during the polycondensation reaction.

(23) An explicit comment on the exact mechanistic aspects of this novel observation needs extensive investigations. In this occasion we note that the exact mechanisms of certain nanoparticle-catalyzed reactions are still not known: for example, oxidation of CO by Au nanoparticles. See ref 3 for a review and: Chen, Y.; Crawford, P.; Hu, P. *Catal. Lett.* **2007**, *119*, 21–28.

(24) Novo, C.; Funston, A. M.; Mulvaney, P. *Nat. Nanotechnol.* **2008**, *3*, 598–602.

(25) (a) Kvítek, L.; Panáček, A.; Soukupová, J.; Kolář, M.; Večeřová, R.; Prucek, R.; Holecová, M.; Zbořil, R. *J. Phys. Chem. C* **2008**, *112*, 5825–5834. (b) Pal, S.; Tak, Y. K.; Song, J. M. *Appl. Environ. Microbiol.* **2007**, *73*, 1712–1720. (c) Sharma, V. K.; Yngard, R. A.; Lin, Y. *Adv. Colloid Interface Sci.* **2009**, *145*, 83–96.

(26) (a) Noghabi, K. A.; Zahiri, H. S.; Yoon, S. C. *Process Biochem.* **2007**, *42*, 847–855. (b) Shahverdi, A. R.; Fakhimi, A.; Shahverdi, H. R.; Minaian, S. *Nanomed. Nanotech. Biol. Med.* **2007**, *3*, 168–171. (c) Ruparelia, J. P.; Chatterjee, A. K.; Duttagupta, S. P.; Mukherji, S. *Acta Biomat.* **2008**, *4*, 707–716. (d) Kora, A. J.; Manjusha, R.; Arunachalam, J. *Mater. Sci. Eng. C* **2009**, *29*, 2104–2109. (e) Guzmán, M. G.; Dille, J.; Godet, S. *World Acad. Sci. Eng. Technol.* **2008**, *43*, 357–364.

AM9005034